TUDelft

Delft University of Technology

Short communication

Influence of ionic liquid anions on electrochemical CO_2 reduction to higher hydrocarbons on sulfur-vacant MoS_2

Eszter Mádai [a,c], Prasaanth Ravi Anusuyadevi [a], Prasad Gonogunta [a], Seyedamirhossein Mohseni Armaki [a], Remco Hartkamp [b,c], Arjan Mol [a], Peyman Taheri [a,c] [iD],*

[a] Department of Materials Science and Engineering, Faculty of Mechanical Engineering, Delft University of Technology, Mekelweg 2, Delft, 2628 CD, The Netherlands
[b] Department of Process and Energy, Faculty of Mechanical Engineering, Delft University of Technology, Leeghwaterstraat 39, Delft, 2628 CB, The Netherlands
[c] e-Refinery Institute, Delft University of Technology, Leeghwaterstraat 39, Delft, 2628 CB, The Netherlands

ARTICLE INFO

ABSTRACT

Molybdenum disulfide (MoS_2) has emerged as a promising electrocatalyst for the electrochemical reduction of CO_2, primarily yielding carbon monoxide. However, product selectivity is known to be highly sensitive to structural features such as edge termination and defect density. In this work, we report the formation of higher hydrocarbons (C_2+ products) enabled by the presence of inherent sulfur vacancies in MoS_2 when combined with various ionic liquids as co-catalysts. While MoS_2 has traditionally shown limited hydrocarbon output, our findings demonstrate for the first time that native defect sites, interacting synergistically with the electrolyte environment, can facilitate the production of significant amounts of C_2+ species. These results provide new insights into defect-mediated catalytic pathways and highlight the importance of electrolyte design in tuning product distribution during CO_2 electroreduction.

1. Introduction & background

The Paris agreement, signed by 196 parties in 2016, targets carbon-neutrality by 2050 [1]. Hence, establishing a carbon-neutral or carbon-negative cycle is one of the primary targets in research and policy. This goal demands the development of viable technologies for carbon capture and utilization to value-added compounds [2]. Consequently, the electrochemical conversion of carbon dioxide (CO_2) to multi-carbon (C_n) species has attracted attention as it presents a viable path to carbon-neutrality [3–5].

Recently, 2D materials emerged as future electrocatalysts for CO_2 reduction reaction (CO_2RR) due to their high surface-to-bulk ratio [6]. Among them, transition metal dichalcogenides (TMDCs) showed great potential [7]. Their layered structure allows the surface-to-bulk ratio to be maximized with exfoliation and their earth-abundance makes them favorable and more cost-effective than precious metals. MoS_2, a prominent member of TMDCs, has garnered significant attention for its remarkable affordability, high tunability and efficiency in electrolysis. Currently, researchers are exploring its potential in the CO_2RR.

MoS_2 shows a great affinity towards the hydrogen evolution reaction (HER) [8,9] which, as a competitive reaction, reduces the CO_2RR efficiency. However, when molybdenum disulfide is aided by 1-ethyl-3-methylimidazolium tetrafluoroborate ([EMIM][BF$_4$]) as a co-catalyst,

it offers a superior selectivity of the CO_2RR to carbon monoxide (CO), reported by Asadi et al. [10,11]. It has been suggested that incorporating a co-catalyst can effectively lower the overpotential and suppress the HER by the ionic liquid (IL) adsorbing onto the catalyst surface, thereby blocking water molecules from accessing it [12]. The catalytic activity towards CO_2RR is attributed to the Mo-terminated edges of MoS_2, where Mo atoms facilitate a continuous electron supply to the attached intermediates, enhancing the reaction efficiency.

Building further on these results, it was shown that doping vertically aligned (VA) MoS_2 with Nb-doping further increases the FE of the CO_2RR towards CO up to 90%, while Ta-doping decreases it due to a suboptimal electronic structure resulting from the binding between the Ta atoms and the host structure [13]. Another study on CO_2RR using single-crystal-terrace MoS_2 electrodes (mechanically exfoliated MoS_2) in 0.1 M Na_2CO_3 aqueous solution established a correlation between edge density and product selectivity [14]. It revealed that increasing the edge density reduces the Faradaic efficiency (FE) for CO_2RR to 1-propanol, the primary product in this case. This suggests that in an aqueous environment, Mo-terminated edges favor HER over CO_2RR, while the activation of basal planes is necessary for producing higher hydrocarbons. Although the HER significantly suppressed the CO_2RR,

---

* Correspondence to: TU Delft - ME - MSE, Mekelweg 2, 2628 CD, Delft, the Netherlands.
 E-mail address: p.taheri@tudelft.nl (P. Taheri).

the authors also identified formate, ethylene glycol, methanol, and t-butanol in trace concentrations alongside 1-propanol.

Based on the available experimental information, density functional theory (DFT) calculations showed the possible pathways of the CO_2RR to CO or C_n products on MoS_2 [15]. As the reaction takes place on the exposed Mo edges, they showed that the d-band center of the Mo atom is much closer to the Fermi level of MoS_2 than for metallic catalysts, such as copper or titanium. Thus, the adsorbed species interact stronger with the Mo atoms. Furthermore, assuming that the intermediates are COOH* and CO*, their formation energies are smaller than those of CO_2 and CO (one of the possible primary products), thus the Mo atoms at the edges also exhibit a strong binding of the intermediates. The reaction pathway towards CO is energetically favorable to the pathway towards C_n products, consistent with findings in prior work [10].

However, while CO serves as a valuable feedstock for various chemical reactions, developing catalysts capable of directly producing a range of higher-carbon products offers significant advantages in terms of market value and energy density [16]. Many catalysts are only able to produce C_1-C_2 products and suffer from stability issues at high potentials [17,18]. Hence, finding a way to achieve higher hydrocarbon products with a stable and active electrocatalyst like MoS_2 is of high interest.

A potential pathway for hydrocarbon production is linked to sulfur vacancies (V_Ss) in the MoS_2 structure. Building on the findings of Francis et al. [14], Kang et al. [19] proposed that the active sites are more likely to reside on the basal plane, based on the observation that an increased edge density correlates with a decrease in the FE towards 1-propanol [14]. The clean basal plane of the MoS_2 is known to be inert; hence, the authors investigated the effect of sulfur vacancies as potential active sites in the basal plane. It is already proved that during the synthesis of MoS_2 films, V_Ss in the basal plane can occur up to 10% as their formation energy is relatively low (1–3 eV dependent on growth conditions) [20] and it has been shown that these V_Ss can act as active sites for the HER [21]. The authors demonstrated through DFT calculations that three sub-gap states, associated with V_Ss, are inherently localized. As a result, these states enable the independent occurrence of electron and proton transfer during the reduction reaction, which otherwise would proceed concurrently. Furthermore, the authors demonstrated that, contrary to previous studies, *OCHO is formed in the initial protonation step instead of *COOH due to the bowl-shape of the V_Ss as it sterically hinders the incorporation of more than one molecule into the vacancy site. Moreover, this new intermediate facilitates the formation pathway of formaldehyde as a C_1 product, a highly reactive chemical. As this new intermediate makes its binding to the active sites (sulfur vacancies) viable, in turn, it also enables subsequent C–C coupling reactions, fostering the formation of higher C_n products.

Despite the theoretical studies on sulfur-vacant MoS_2 (V_S-MoS_2) as a catalyst for the electrochemical CO2 reduction reaction, the experimental influence of sulfur vacancies on product distribution remains unaddressed. Additionally, while the role of [EMIM][BF$_4$] as co-catalysts has been investigated, comparative studies involving different anions, beyond the commonly used [EMIM][BF4], are lacking. As Asadi et al. emphasized the importance of the [EMIM]$^+$ cation of the ionic liquids [10], because of the complex formation and the potential physisorption on the surface of the MoS_2 catalyst. Furthermore, results from the literature have suggested that along [EMIM][BF$_4$], 1-ethyl-3-methilimidazolium trifluoromethanesulfonate ([EMIM][Otf]) could be a possible co-catalyst to promote the CO_2RR over the HER [21]. Hence, in this work, we experimentally study V_S-MoS2 nanoflakes in the CO2RR using two ionic liquids, [EMIM][BF$_4$] and [EMIM][Otf], which share the [EMIM]$^+$ cation but differ in their anions. By comparing the performance of [EMIM][BF$_4$] and [EMIM][Otf], we aim to establish criteria for the key physicochemical properties an optimal co-catalyst should possess.
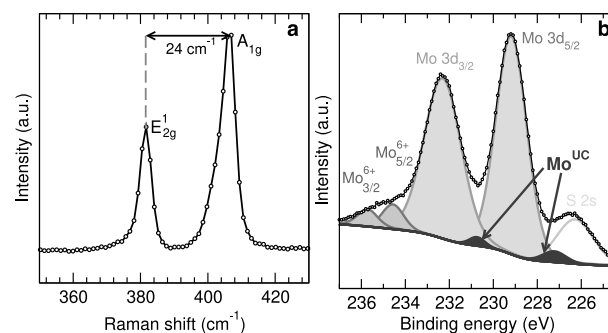

Fig. 1. (a) Raman spectrum of the V_S-MoS_2 catalyst showing the two characteristic peaks, E^1_{2g} and A_{1g} of the material, (b) Fitted Mo 3d5 XPS spectrum of the V_S-MoS_2 catalyst showing the different valence states of the Mo atoms in the structure.

2. Results & discussion

For the working electrodes MoS_2 nanopowder (Sigma-Aldrich, 90 nm average particle size) was mixed with carbon black (Fischer Scientific) and polyvinyl alcohol and then dropcasted on glassy carbon substrates. The MoS_2-based electrode was prepared following the same procedure described in our previous work [22]. The commercial MoS_2 nanopowder inherently contains a baseline concentration of sulfur vacancies, as commonly observed for this material due to its synthesis and storage history [20]. Mild sonication during dispersion can additionally create single-sulfur defects, while subsequent electrochemical activation under reductive potentials further stabilizes these sites. Comprehensive surface and elemental analyses of the same material, including SEM, XRD, EDS, and XPS, are reported in our earlier publication, confirming the structural integrity and the presence of intrinsic sulfur vacancies. Fig. 1(a) presents the Raman spectrum of the MoS_2 nanoflakes, where the separation between the two main characteristic peaks (E^1_{2g} and A_{1g}) is 24 cm^{-1}, compared to 21 cm^{-1} for the pristine MoS_2 [23].

This larger separation shows the formation of monosulfur vacancies in the MoS_2 structure [24,25]. X-ray photoelectron spectroscopy (XPS) further confirmed the presence of these monosulfur vacancies. Fig. 1(b) shows the fitted Mo 3d5 spectrum of the V_S-MoS_2 catalyst, where the two main peaks were identified as the Mo $3d^{3/2}$ and $3d^{5/2}$ peaks at 229.1 eV and 232.4 eV, respectively. Furthermore, Mo^{6+} was identified due to possible oxidation during the sonication process; and undercoordinated Mo sites (Mo^{UC}) were also found, which confirms the presence of the monosulfur vacancies [25–27]. It is well established that sulfur vacancies modify the electronic structure of MoS_2 by introducing defect states near the Fermi level, which enhance electron density and facilitate charge transport across the basal planes. As demonstrated in our previous work [22], a higher sulfur-vacancy concentration correlates with improved electronic conductivity, thereby enabling more efficient electron transfer to adsorbed CO_2 intermediates during the reduction process. The SEM image in Figure S2 shows the differently oriented V_S-MoS_2 nanoflakes at the surface of the catalyst. The image shows that mainly the basal planes of the V_S-MoS_2 nanoflakes were exposed on the surface, giving the opportunity for the activation of these planes.

To see the effect of monosulfur vacancies in the V_S-MoS_2 structure on the product distribution of the electrochemical CO_2 reduction, two different ionic liquids were used as co-catalysts to promote the CO_2RR. They were each used as 30 vol% IL mixed with 70 vol% deionized water and purged with CO_2 gas.

Fig. 2 shows the linear sweep voltammetry curves obtained with the two different co-catalysts. For [EMIM][BF$_4$], a small reduction well was seen at 0.9 V vs RHE, while no reduction well was detected with [EMIM][Otf]. The voltammetric response of the MoS_2 electrode in CO_2-saturated 30 vol% [EMIM][BF$_4$] and 70 vol% H_2O (Fig. 2) exhibits a broad reduction feature centered near −0.9V vs. RHE.
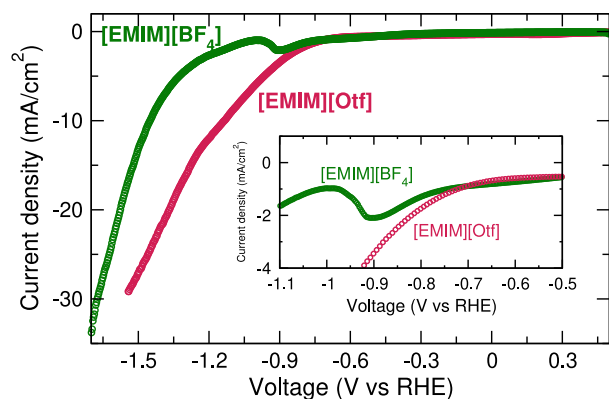
Fig. 2. Linear sweep voltammetry curves of the MoS_2 catalyst in [EMIM][BF_4]-water mixture (green) and [EMIM][Otf]-water (red) mixture.

Fig. 3. Faradaic efficiencies and product distribution of the CO_2RR on MoS_2 with the two different 30 vol% ILs and 70 vol% water mixtures as co-catalysts at -0.9 V vs RHE.

Although the current density is modest (≈ 2 mA cm^{-2}), chronoamperometric electrolysis performed at this potential produces C2+ products with a high combined Faradaic efficiency, confirming the Faradaic nature of the process. The weak appearance of the feature is therefore attributed to the relatively low conductivity and high viscosity of the ionic-liquid–containing electrolyte, rather than to capacitive effects. Chronoamperometry data for both ionic-liquid systems have been added to the Supplementary Materials (Figure S5), showing that the MoS_2 electrodes remain stable during 60 min of continuous electrolysis.

The CO_2 reduction efficiency was measured with gas chromatography and then the FE was calculated for both ionic liquids, which is shown in Fig. 3. When [EMIM][BF_4] was used as a co-catalyst, a wide range of hydrocarbons (CH_4, C_2H_6, i-H_5C_{12} and C_6H_{10}) was produced with some hydrogen as a side-product. Out of this range of hydrocarbons, isopentane emerged as the main product with 44% FE. On the other hand, when [EMIM][Otf] is used as a co-catalyst, hydrogen is the only product that is detected.

A crucial feature of MoS_2 is the deviation from the linear scaling relations, where the adsorption energy scales with the concentration of the intermediate [28]. It has been shown that for different transition-metal catalysts, the adsorption energies of the COOH* and the CHO* intermediates are strongly correlated with the adsorption energy of CO* [29]. In the case of V_S-MoS_2, the exposed transition metal Mo atoms are the active sites for the CO_2RR. Hence, these linear scaling relations between the reaction intermediates of the CO_2RR also strongly affect the reduction activity of the transition-metal catalysts [30]. These relations also suggest that the stability of COOH* and CHO* is strongly dependent on CO*, whereas a criterion for the catalyst would be to stabilize COOH* and CHO* better than CO*. In this regard, it was also shown that MoS_2 and $MoSe_2$ (both pristine and doped) break the scaling relations by binding the COOH*and CHO* more strongly than the CO*/CO, leading to a higher selectivity [31]. This phenomenon is attributed to the presence of S and Se atoms on the edges of the catalysts, which have a higher binding affinity towards the other intermediates than towards CO. On the other hand, this higher affinity towards the binding of these intermediates also implies the affinity towards C_n (n> 1) products, as to produce longer chain hydrocarbons in addition to the expected selectivity, as it was also shown by Francis et al. [14] and our experiments. Hence, the synergy of using V_S-MoS_2 as a catalyst originates from two factors: (1) that it inherently breaks the linear scaling relations between the reaction intermediates [28] and (2) it exposes transition metal centers as active sites for the CO_2RR due to the sulfur vacancies [25,32]. Furthermore, as the SEM images show thin, overlapping MoS_2 nanoflakes that form compact films, resulting in limited edge exposure relative to the total surface area. Thus, the high selectivity towards C_2^+ products observed here differs from the C_1-dominated pathways typically associated with MoS_2 edge sites [10,13], suggesting that basal-plane defects govern the observed activity.
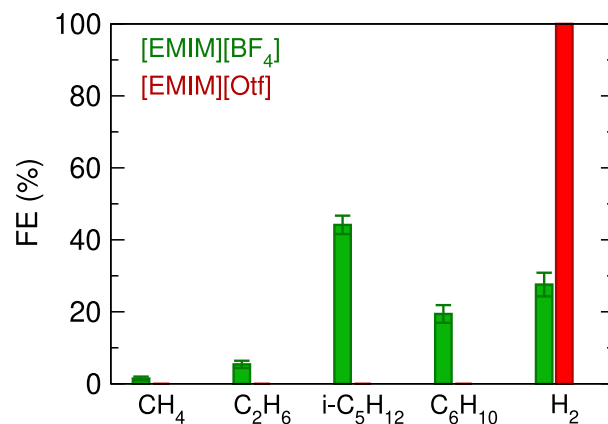
To assess the origin of the difference between the product distributions when the different ionic liquids were used as co-catalysts, XPS measurements were done on the exposed V_S-MoS_2 catalysts. Fig. 4(a) shows the fitted C 1s spectrum of the V_S-MoS_2 catalyst exposed prior to [EMIM][BF_4]. Two subpeaks were identified, one peak at 283.5 eV, which comprises the adventitious carbon peak (284.4 eV, possibly due to device contamination) and the C=C bonding from the IL [33], and a C–N bonding peak at 285.5 eV [34]. The latter peak could originate from the physisorbed [EMIM]$^+$ cation, as the ab-initio molecular dynamics simulations of Asadi et al. indicated [10]. Fig. 4(b) presents the deconvoluted C 1s spectrum of the V_S-MoS_2 catalyst exposed to [EMIM][Otf]. During the deconvolution, 6 peaks were identified: at 282.5 a small peak which shows the presence of metal carbides on the surface, the adventitious carbon and the C=C bond from the IL at 283.5 eV, the C–N bonding at 285.5 eV showing the presence of the [EMIM]$^+$ cation on the surface, a small C-OH peak at 286.5 eV and CF_2 and CF_3 peaks at 291 eV and 293 eV, respectively [33].

The presence of the metal carbide, CF_2 and CF_3 peaks leads to the assumption that the [Otf]- anion of the ionic liquid is chemically bound to the undercoordinated Mo sites of the V_S-MoS_2 catalyst. As the [Otf]$^+$ anion possesses a CF_3 group, the small peak of the CF_3 group and the larger peak of the CF_2 group and the presence of the metal-carbide peak suggests that the anion of the ionic liquid is chemically bound to the Mo atom. This binding process is likely to occur on the Mo atoms that are exposed on the surface due to the presence of the sulfur vacancies. Therefore, as the active sites of the electrochemical CO_2RR are blocked, H_2 was the only product measured.

The high-resolution F 1s and B 1s spectra (Supplementary Materials, Figure S7 a and b) show distinct spectral features depending on the ionic-liquid anion. For [EMIM][BF_4], the F 1s signal appears at 684 eV, consistent with B–F bonding and the B 1s peak characteristic of BF_4^-, confirming the presence of this anion near the catalyst surface. In contrast, for [EMIM][Otf], the F 1s signal is shifted to 688 eV, indicative of organic-fluoride species, which corresponds to the C–F component observed in the C 1s region. These findings support the proposed surface passivation effect of the [Otf]$^-$ anion.

Fig. 5 compares the Faradaic efficiencies of CO_2RR and HER when [EMIM][BF_4] is used as co-catalyst between this work (V_S-MoS_2), and other data that can be found in the literature, namely the Mo-edge terminated bulk MoS_2 (Asadi et al.) and VA-$Nb_{0.05}Mo_{0.95}S_2$ (Abbasi et al.) catalysts. For the V_S-MoS_2 catalyst, the different hydrocarbon products of the CO_2RR are added up, reaching 70% overall FE for the CO_2RR, which is lower than the bulk MoS_2 and the VA-$Nb_{0.05}Mo_{0.95}S_2$ catalysts, with 98% and 82% FEs, respectively. Improving the FE of the V_S-MoS_2 can potentially originate from two sources: (1) improving
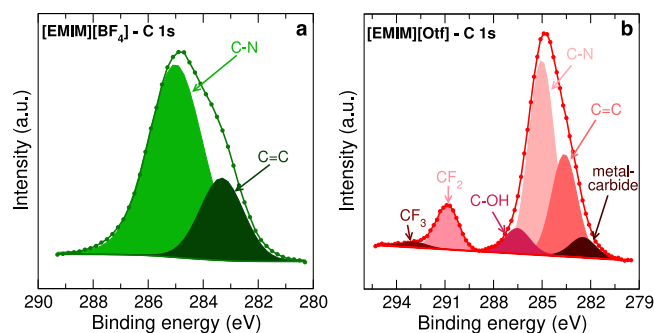
Fig. 4. Normalized C 1s XPS spectra of VS-MoS2 catalyst exposed to [EMIM][BF4] **(a)** and to [EMIM][Otf] **(b)**.

the electronic properties of the V_S-MoS_2 catalyst and/or (2) finding a more suitable co-catalyst in the form of different ionic liquids.

Abbasi et al. showed that doping MoS_2 with different metals is a potential way to change its material properties and through that, influence the FE of CO_2RR. However, the dopant must be carefully selected, as it can also negatively impact the efficiency of the CO_2RR [13]. To avoid this potentially negative influence on the efficiency, another path to change the electronic properties is through utilizing the layered 2-dimensional structure of MoS_2 by intercalating ions into the interlayer space. The conductivity of MoS_2 can be increased through electron donation from the intercalants [35,36], which can potentially influence the product distribution and the FE of the CO_2RR. Regarding the effect of the co-catalyst, we experimentally proved that the $[EMIM]^+$ cation is indeed important for creating an environment that favors the CO_2RR over the HER at the catalyst surface. However, using $[EMIM][BF_4]$ as a co-catalyst also has the hazardous aspect that the $[BF_4]$- anion can hydrolyze to HF [10]. This aspect compromises the potential for scaling up the process. Furthermore, the capacity of $[EMIM][BF_4]$ to absorb CO_2 is much lower than that of other imidazolium-based ionic liquids [37]. We also showed that not only does the cation of the ionic liquid matter, but also the anion, as it can potentially poison the catalyst. Taking all these criteria into account, imidazolium-based acetates seem to be an ideal choice as a next step for co-catalyst selection, due to their high affinity towards CO_2 absorption, stable structure and lack of potential side-reactions [38].

3. Conclusions

We experimentally demonstrated that introducing sulfur vacancies into the basal plane of MoS_2 enhances its catalytic activity for the electrochemical CO_2 reduction reaction, enabling the formation of multi-carbon (C_n) products. However, the presence of V_S alone results in a broad product distribution with limited selectivity. To further understand the catalytic environment, we investigated the role of the ionic liquid co-catalyst by comparing $[EMIM][BF_4]$ and $[EMIM][Otf]$, which share the $[EMIM]^+$ cation but differ in their anions. Our results reveal that, in addition to the crucial contribution of the $[EMIM]^+$ cation, the choice of anion significantly affects catalytic performance by influencing surface interactions. Specifically, chemically aggressive anions may bind to the catalyst surface and deactivate it. Hence, the criteria for an efficient co-catalyst are the use of imidazolium-based ionic liquids with anions that are less reactive and possess a structure enabling high CO_2 uptake (such as acetates), thereby enhancing CO_2 availability. Moreover, safety considerations are critical, as certain anions, such as BF_4^-, may lead to hazardous by-products, including HF. These findings address key experimental gaps in the understanding of sulfur-vacant MoS_2 catalysts and ionic liquid composition in CO_2RR, and they provide a foundation for the rational design of more effective and selective catalyst–co-catalyst systems.
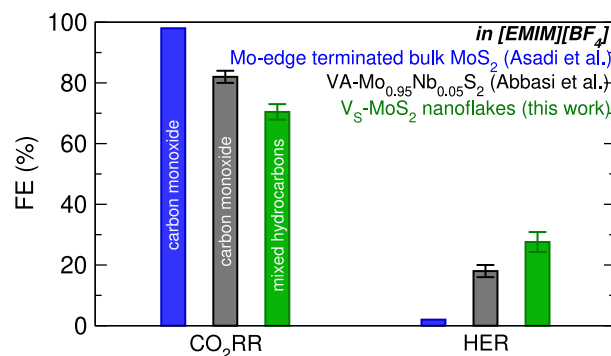

Fig. 5. Comparison of CO_2RR FE of V_S-MoS_2 nanoflakes with Mo-edge terminated bulk MoS_2 and VA-$Nb_{0.05}Mo_{0.95}S_2$ with $[EMIM][BF_4]$ as co-catalyst. For comparison data was extracted from Abbasi et al. [13] and Asadi et al. [10].

CRediT authorship contribution statement

Eszter Mádai: Writing – review & editing, Writing – original draft, Visualization, Validation, Software, Methodology, Investigation, Formal analysis, Data curation, Conceptualization. **Prasaanth Ravi Anusuyadevi:** Writing – review & editing, Validation, Methodology, Investigation, Formal analysis. **Prasad Gonogunta:** Validation, Methodology, Investigation. **Seyedamirhossein Mohseni Armaki:** Methodology, Investigation. **Remco Hartkamp:** Writing – review & editing, Visualization, Supervision. **Arjan Mol:** Writing – review & editing, Supervision. **Peyman Taheri:** Writing – review & editing, Supervision, Project administration, Funding acquisition.

Appendix A. Supplementary data

Supplementary material related to this article can be found online at https://doi.org/10.1016/j.apcato.2025.207083.

Data availability

Data will be made available on request.

References

[1] M.-C.C. Segger, Advancing the paris agreement on climate change for sustainable development, Camb. Int. Law J. 5 (2016) 202–237.

[2] G. Garcia-Garcia, M.C. Fernandez, K. Armstrong, S. Woolass, P. Styring, Analytical review of life-cycle environmental impacts of carbon capture and utilization technologies, ChemSusChem 14 (2021) 995–1015.

[3] M.G. Kibria, J.P. Edwards, C.M. Gabardo, C.-T. Dinh, A. Seifitokaldani, D. Sinton, E.H. Sargent, Electrochemical CO2 reduction into chemical feedstocks: from mechanistic electrocatalysis models to system design, Adv. Mater. 31 (2019) 1807166.

[4] T. Ahmad, S. Liu, M. Sajid, K. Li, M. Ali, L. Liu, W. Chen, Electrochemical CO2 reduction to C2+ products using cu-based electrocatalysts: A review, Nano Res. Energy 1 (2022) e9120021.

[5] K. Li, S. Zhang, X. Zhang, S. Liu, H. Jiang, T. Jiang, C. Shen, Y. Yu, W. Chen, Atomic tuning of single-atom Fe–N–C catalysts with phosphorus for robust electrochemical CO2 reduction, Nano Lett. 22 (2022) 1557–1565.

[6] X. Duan, J. Xu, Z. Wei, J. Ma, S. Guo, S. Wang, H. Liu, S. Dou, Metal-free carbon materials for CO2 electrochemical reduction, Adv. Mater. 29 (2017) 1701784.

[7] F.-Y. Gao, Z.-Z. Wu, M.-R. Gao, Electrochemical CO2 reduction on transition-metal chalcogenide catalysts: recent advances and future perspectives, Energy & Fuels 35 (2021) 12869–12883.

[8] D. Voiry, M. Salehi, R. Silva, T. Fujita, M. Chen, T. Asefa, V.B. Shenoy, G. Eda, M. Chhowalla, Conducting MoS2 nanosheets as catalysts for hydrogen evolution reaction, Nano Lett. 13 (2013) 6222–6227.

[9] C. Tsai, H. Li, S. Park, J. Park, H.S. Han, J.K. Nørskov, X. Zheng, F. Abild-Pedersen, Electrochemical generation of sulfur vacancies in the basal plane of MoS2 for hydrogen evolution, Nat. Commun. 8 (2017) 15113.

[10] M. Asadi, B. Kumar, A. Behranginia, B.A. Rosen, A. Baskin, N. Repnin, D. Pisasale, P. Phillips, W. Zhu, R. Haasch, et al., Robust carbon dioxide reduction on molybdenum disulphide edges, Nat. Commun. 5 (2014) 4470.

[11] M. Asadi, K. Kim, C. Liu, A.V. Addepalli, P. Abbasi, P. Yasaei, P. Phillips, A. Behranginia, J.M. Cerrato, R. Haasch, et al., Nanostructured transition metal dichalcogenide electrocatalysts for CO2 reduction in ionic liquid, Science 353 (2016) 467–470.

[12] B.A. Rosen, J.L. Haan, P. Mukherjee, B. Braunschweig, W. Zhu, A. Salehi-Khojin, D.D. Dlott, R.I. Masel, In situ spectroscopic examination of a low overpotential pathway for carbon dioxide conversion to carbon monoxide, J. Phys. Chem. C 116 (2012) 15307–15312.

[13] P. Abbasi, M. Asadi, C. Liu, S. Sharifi-Asl, B. Sayahpour, A. Behranginia, P. Zapol, R. Shahbazian-Yassar, L.A. Curtiss, A. Salehi-Khojin, Tailoring the edge structure of molybdenum disulfide toward electrocatalytic reduction of carbon dioxide, ACS Nano 11 (2017) 453–460.

[14] S.A. Francis, J.M. Velazquez, I.M. Ferrer, D.A. Torelli, D. Guevarra, M.T. McDowell, K. Sun, X. Zhou, F.H. Saadi, J. John, et al., Reduction of aqueous CO2 to 1-propanol at MoS2 electrodes, Chem. Mater. 30 (2018) 4902–4908.

[15] Y. Xie, X. Li, Y. Wang, B. Li, L. Yang, N. Zhao, M. Liu, X. Wang, Y. Yu, J.-M. Liu, Reaction mechanisms for reduction of CO2 to CO on monolayer MoS2, Appl. Surf. Sci. 499 (2020) 143964.

[16] S. Verma, S. Lu, P.J. Kenis, Co-electrolysis of CO2 and glycerol as a pathway to carbon chemicals with improved technoeconomics due to low electricity consumption, Nat. Energy 4 (2019) 466–474.

[17] X. Zhi, Y. Jiao, Y. Zheng, A. Vasileff, S.-Z. Qiao, Selectivity roadmap for electrochemical CO2 reduction on copper-based alloy catalysts, Nano Energy 71 (2020) 104601.

[18] M.T. Tang, H. Peng, P.S. Lamoureux, M. Bajdich, F. Abild-Pedersen, From electricity to fuels: descriptors for C1 selectivity in electrochemical CO2 reduction, Appl. Catal. B: Environ. 279 (2020) 119384.

[19] S. Kang, S. Han, Y. Kang, Unveiling electrochemical reaction pathways of CO2 reduction to cn species at s-vacancies of MoS2, ChemSusChem 12 (2019) 2671–2678.

[20] G. Li, D. Zhang, Q. Qiao, Y. Yu, D. Peterson, A. Zafar, R. Kumar, S. Curtarolo, F. Hunte, S. Shannon, et al., All the catalytic active sites of MoS2 for hydrogen evolution, J. Am. Chem. Soc. 138 (2016) 16632–16638.

[21] A. Hailu, S.K. Shaw, Efficient electrocatalytic reduction of carbon dioxide in 1-ethyl-3-methylimidazolium trifluoromethanesulfonate and water mixtures, Energy & Fuels 32 (2018) 12695–12702.

[22] E. Mádai, P.R. Anusuyadevi, P. Gonugunta, A.M. Armaki, A. Mol, P. Taheri, R. Hartkamp, Effects of alkali metal intercalation on structural and electronic properties of molybdenum disulfide, Appl. Surf. Sci. 714 (2025) 164284.

[23] H. Li, Q. Zhang, C.C.R. Yap, B.K. Tay, T.H.T. Edwin, A. Olivier, D. Baillargeat, From bulk to monolayer MoS2: Evolution of raman scattering, Adv. Funct. Mater. 22 (2012) 1385–1390.

[24] Q. Wang, X. Li, X. Ma, Z. Li, Y. Yang, Activation of the MoS2 basal plane to enhance co hydrogenation to methane activity through increasing s vacancies, ACS Appl. Mater. & Interfaces 14 (2022) 7741–7755.

[25] L. Li, Z. Qin, L. Ries, S. Hong, T. Michel, J. Yang, C. Salameh, M. Bechelany, P. Miele, D. Kaplan, et al., Role of sulfur vacancies and undercoordinated Mo regions in MoS2 nanosheets toward the evolution of hydrogen, ACS Nano 13 (2019) 6824–6834.

[26] X. Zhang, S. Wang, C.-K. Lee, C.-M. Cheng, J.-C. Lan, X. Li, J. Qiao, X. Tao, Unravelling the effect of sulfur vacancies on the electronic structure of the MoS2 crystal, Phys. Chem. Chem. Phys. 22 (2020) 21776–21783.

[27] H. Fei, R. Liu, J. Wang, T. Guo, Z. Wu, D. Wang, F. Liu, Targeted modulation of competitive active sites toward nitrogen fixation via sulfur vacancy engineering over MoS2, Adv. Funct. Mater. 33 (2023).

[28] Y. Ji, J.K. Nørskov, K. Chan, Scaling relations on basal plane vacancies of transition metal dichalcogenides for CO2 reduction, J. Phys. Chem. C 123 (2019) 4256–4261.

[29] A.A. Peterson, J.K. Nørskov, Activity descriptors for CO2 electroreduction to methane on transition-metal catalysts, J. Phys. Chem. Lett. 3 (2012) 251–258.

[30] P. Mano, T. Jitwatanasirikul, T. Roongcharoen, K. Takahashi, S. Namuangruk, Tuning covalent bonding of single transition metal atom doped in s vacant MoS2 for catalytic CO2 reduction reaction product selectivity, Appl. Surf. Sci. 688 (2025) 162339.

[31] K. Chan, C. Tsai, H.A. Hansen, J.K. Nørskov, Molybdenum sulfides and selenides as possible electrocatalysts for CO2 reduction, ChemCatChem 6 (2014) 1899–1905.

[32] H. Li, C. Tsai, A.L. Koh, L. Cai, A.W. Contryman, A.H. Fragapane, J. Zhao, H.S. Han, H.C. Manoharan, F. Abild-Pedersen, et al., Activating and optimizing MoS2 basal planes for hydrogen evolution through the formation of strained sulphur vacancies, Nat. Mater. 15 (2016) 48–53.

[33] K. Dave, K.H. Park, M. Dhayal, Two-step process for programmable removal of oxygen functionalities of graphene oxide: functional, structural and electrical characteristics, RSC Adv. 5 (2015) 95657–95665.

[34] J. Kalaiyarasi, K. Pandian, S. Ramanathan, S.C. Gopinath, Graphitic carbon nitride/graphene nanoflakes hybrid system for electrochemical sensing of dna bases in meat samples, Sci. Rep. 10 (2020) 12860.

[35] R. Somoano, V. Hadek, A. Rembaum, Alkali metal intercalates of molybdenum disulfide, J. Chem. Phys. 58 (1973) 697–701.

[36] X. Wang, X. Shen, Z. Wang, R. Yu, L. Chen, Atomic-scale clarification of structural transition of MoS2 upon sodium intercalation, ACS Nano 8 (2014) 11394–11400.

[37] C. Wang, H. Luo, X. Luo, H. Li, S. Dai, Equimolar CO2 capture by imidazolium-based ionic liquids and superbase systems, Green Chem. 12 (2010) 2019–2023.

[38] J.D. Watkins, A.B. Bocarsly, Direct reduction of carbon dioxide to formate in high-gas-capacity ionic liquids at post-transition-metal electrodes, ChemSusChem 7 (2014) 284–290.